Dependance of the structural and physical properties of $Tl_{1-y}Fe_{2-z}(Se_{1-x}S_x)_2$ with isovalent substitution of Se by S: decrease of $T_{Néel}$ with S content

P. Toulemonde,[*] D. Santos-Cottin, Ch. Lepoittevin, P. Strobel, and J. Marcus

Institut Néel, CNRS and Université Joseph Fourier,
25 avenue des Martyrs, BP 166, F-38042 Grenoble cedex 9, France.
(Dated: November 10, 2018)

The effect of selenium substitution by sulfur or tellurium in the $Tl_{1-y}Fe_{2-z}Se_2$ antiferromagnet was studied by x-ray and electron diffraction, magnetization and transport measurements. The full solid solution series $Tl_{1-y}Fe_{2-z}(Se_{1-x}X_x)_2$ was synthesized for X=Se and up to x=0.5 for X=Te, using the sealed tube technique. No superconductivity was found down to 4.2K in the case of sulfur despite that the optimal crystallographic parameters, determined by Rietveld refinements, are reached in the series (i.e. the Fe-(Se,S) interplane height and (Se,S)-Fe-(Se,S) angle for which the critical superconducting transition T_c is usually maximal in pnictides). Compounds substituted with tellurium, at least up to x=0.25, show superconducting transitions but probably due to tetragonal Fe(Se,Te) impurity phase. Transmission electron microscopy confirmed the existence of ordered iron vacancies network in S-substituted samples (in tetragonal $\sqrt{5}$ a $\times\sqrt{5}$ a $\times$ c superstructure ($I4/m$) or in orthorhombic $\sqrt{2}$ a $\times 2\sqrt{2}$ a $\times$ c supercell ($Ibam$)). The Néel temperature (T_N) indicating the onset of antiferromagnetism order decreases from 450K in the selenide (x=0) to 330K in the sulfide (x=1). We finally demonstrate a direct linear relationship between $T_{Néel}$ and the Fe-(Se,S) bond length (or Fe-(Se,S) height).

I. INTRODUCTION

After the discovery of superconductivity in iron-based superconductors, i.e. in pnictides and chalcogenides, numerous families were found, at least five families for arsenides with superconducting transition up to $T_c = 55$ K. In chalogenides, superconductivity was first found in the "11" family ($Fe_{1+y}(Te_{1-x}Ch_x)$) with Ch=Se or S, and recently in a second family $AFe_{2-y}Se_2$ ("122" selenide) with A=K[1], Rb, Cs (or Tl/Rb, Tl/Cs) showing T_c around 30 K, i.e. close to the maximum value measured for FeSe under high pressure[2–4]. A related compound is $TlFe_{2-y}Se_2$, which was firstly synthesized and studied 25 years ago by Haggstrom et al.[5]. This compound is antiferromagnetic with a high Néel temperature around T_N=450K, i.e. in the range of T_N values measured for alkaline intercalated 122 selenides[6].

In iron-based superconductors, superconductivity can be induced by simple isovalent substitution of the pnictogen or chalcogen, for example by substitution of As by P in LnFeAsO (Ln=La,Ce,Pr,Nd,Sm...) ("1111") or "122" arsenides or of Te by Se in the Fe_{1+y}Te telluride. The present work follows the same approach to search for superconductivity in thallium-122 selenide (" Tl-122") by substitution of selenium by sulfur. In addition, this substitution may allow to approach the structural conditions where the highest Tc's are reached in this structural family, i.e. either a Fe-Se bond length around 1.41 Å[7] (in the FeSe system under high pressure) or Ch-Fe-Ch bond angles corresponding to a regular $FeCh_4$ tetrahedron (in Fe-As systems)[8].

During this study we became aware of an investigation of the $K_{1-z}Fe_{2-y}(Se_{1-x}S_x)_2$ series by Lei et al.[9]. In the potassium system, the $x = 0$ end member is already superconducting (T_c=33K) and superconductivity disappears with increasing x(S). This may be related to (i) a decrease in iron non-stoichiometry (i.e. the compound contains less iron vacancies), (ii) an increase in $FeCh_4$ tetrahedron distortion[9].

In this article we study the structural trends vs. sulfur content in the $Tl_{1-y}Fe_{2-z}(Se_{1-x}S_x)_2$ series. Contrary to the alkaline-122 systems, the selenium-only and endmember is known to present no superconductivity. We will show in this article that all sulfur-substituted compositions remain antiferromagnetic above room temperature, and that their Néel temperature decreases linearly with decreasing Fe-Ch bond length.

II. EXPERIMENTAL

$Tl_{1-y}Fe_{2-z}(Se_{1-x}S_x)_2$ samples ("Tl-122") were synthesized using the sealed tube technique as reported elsewhere for $Fe_{1+\delta}(Te_{1-x}Se_x)$[10,11]. Starting materials were commercial Fe pieces (Alfa Aesar, 98%), Tl pieces (Alfa Aesar, 98%), Se chips (Alfa Aesar, 98%) and FeS (Alfa, 99.9%). Precursors with nominal composition $Tl_{0.8}Fe_{1.5}(Se_{1-x}S_x)_2$ were placed in an alumina crucible which was introduced in a quartz tube and sealed under vacuum. The heat treatment constituted of a first heating ramp at 100 ˚C/h up to 700 ˚C followed by a plateau for 12 hours at this temperature; then the samples were slow cooled at 5 ˚C/h to 280 ˚C and maintained at this temperature for 24h, then furnace-cooled. We have also tried the substitution of Se by Te (up to x=0.5) using Te pieces as precursor and a similar temperature profile.

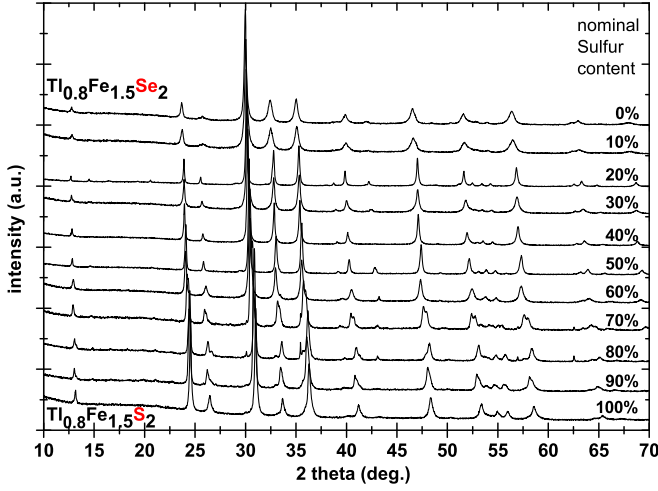X-ray diffraction (XRD) patterns were collected at room temperature using a Bruker D8 powder diffrac-

FIG. 1: XRD patterns (λ = 1.5406 Å) of $Tl_{1-y}Fe_{2-z}(Se_{1-x}S_x)_2$ samples for $0 \leq x \leq 1$. Nominal compositions (at. % S) are indicated.

FIG. 2: Selected low 2-theta region of the XRD patterns of x=0.2 and x=0.6 $Tl_{1-y}Fe_{2-z}(Se_{1-x}S_x)_2$ samples (λ = 1.5406 Å). Supercell weak reflections related to the tetragonal $\sqrt{5}$ a $\times \sqrt{5}$ a $\times$ c (Miller indices labelled "t") or orthorhombic $\sqrt{2}$ a $\times 2\sqrt{2}$ a $\times$ c (labelled "o") superstructures are indicated.

tometer working in Bragg-Brentano geometry at the wavelength $\lambda_{Cu,\ K\alpha1}$ = 1.54056 Å from 2θ = 10 to 90° with a step of 0.032°.

Electron diffraction (ED) studies combined with quantitative energy dispersive spectroscopy (EDS) microanalysis were carried out using a Philips CM 300 transmission electron microscope (TEM), operating at 300 kV, equipped with a +/- 30° double tilt sample holder. Specimens were prepared by crushing a small portion of sample in an agate mortar containing ethanol in order to obtain a powder with particles as thin as possible. Then a droplet of the mixture was deposited on a copper grid with a holey carbon film, in order to obtain an homogeneous particles distribution.

Transport measurements were carried out using the four point contacts technique down to liquid helium temperature. Magnetization of selected samples were measured at low (down to 4.2K) and high temperature (up to 600K) using a home-made magnetometer with a resolution of 5.10^{-6} A.m^2 and with magnetic field up to 6T.

III. RESULTS AND DISCUSSION

A. Powder x-ray diffraction

Figure 1 shows the powder x-ray diffraction (XRD) patterns of polycrystalline $Tl_{1-y}Fe_{2-z}(Se_{1-x}S_x)_2$ samples for nominal sulfur contents from 0 to 100%. All peaks can be indexed in the tetragonal space group $I4/mmm$ found for $AEFe_2As_2$ (AE=Ba,Sr,Ca) arsenides and used originally by Guo et al.[1] for their superconducting KFe_2Se_2 selenide. This tetragonal structure is drawn in the right part of fig. 3. A slight modification of the
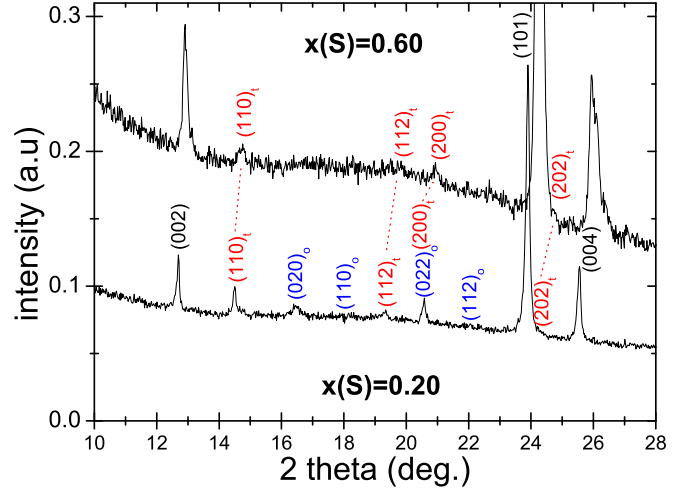
initial nominal composition Tl:Fe:Ch=0.8:1.5:2 induces the emergence of the tetragonal $Fe(Se_{1-x}S_x)$ secondary phase.

In addition, for some sulfur contents, we clearly observe very weak reflections (near the detection limit) at low angle. These supplementary Bragg peaks can be indexed in supercells derived from the original $I4/mmm$ lattice. If a and c represent the subcell parameters, two superstructures were found in the present study: a tetragonal $\sqrt{5}$ a $\times \sqrt{5}$ a $\times$ c one ($I4/m$ space group) and an orthorhombic $\sqrt{2}$ a $\times 2\sqrt{2}$ a $\times$ c one ($Ibam$). This superstructures are due to iron vacancy ordering observed for z=0.4 and z=0.5 by Sabrowksy et al. 25 years ago in $TlFe_{2-z}S_2$ sulfides[12], and confirmed very recently in the new alkaline-based selenides $AFe_{2-z}Se_2$ (A=K,Rb,Cs)[6,14–17] but also in the thallium-based one[13]. An enlargement of the low 2-theta region of the XRD patterns for x=0.2 and x=0.6 (fig. 2) shows for instance that the x=0.2 sample contains both supercells. In contrast, for x=0.6 only the satellite peaks of the $\sqrt{5}$ a $\times \sqrt{5}$ a $\times$ c supercell are found. This interpretation is confirmed by electron diffraction (see below). Further XRD analyses were performed in the average $I4/mmm$ space group, because supercell reflections are extremely weak (near the detection level of our diffraction setup).

Concerning the tellurium-substituted $Tl_{1-z}Fe_{2-y}(Se_{1-x}Te_x)_2$, the synthesis of phase pure samples is more difficult. Above x(Te)=0.2 the sample contains secondary phases: the tetragonal form of $Fe(Te_{1-x}Se_x)$, and $FeTe_2$ and Tl_5Te_3 tellurides. We will not discuss in details these samples in this paper.

An enlargement of two regions of the XRD patterns around (004) and (200) reflections shows a continuous
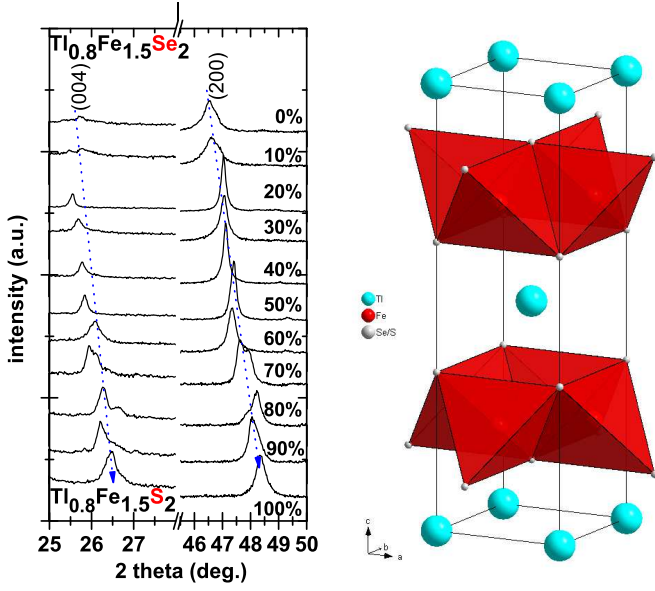
FIG. 3: Left: Selected 2-theta regions of the XRD patterns in the $Tl_{1-y}Fe_{2-z}(Se_{1-x}S_x)_2$ series ($\lambda = 1.5406$ Å) showing the 2 theta shift of (004) and (200) reflections, corresponding to the shrinkage of the lattice with x(S) increase. Right: Tl-122 structure in the $I4/mmm$ space group (i.e. with iron vacancies not ordered).

FIG. 4: Refined lattice parameters in the $Tl_{1-y}Fe_{2-z}(Se_{1-x}X_x)_2$ series with X=S or Te (from Rietveld refinement of the XRD patterns) as a function of S/Te substitution level. Values from literature are taken from ref.[5] for the pure selenide (x=0) and ref.[21] for the pure sulfide (x=1).

shift to higher angle with sulfur content (Figure 3). This corresponds to a decrease of both lattice parameters of the Tl-122 lattice with increasing x(S). The evolution of cell parameters with sulfur content, determined from Rietveld refinement of XRD patterns is displayed in figure 4. The decrease observed here (from a ~ 3.88 Å and c ~ 14 Å for x=0 to a ~ 3.75 Å and c ~ 13.4 Å for x=1) is similar in amplitude to that reported in the potassium $K_{1-y}Fe_{2-z}(Se_{1-x}S_x)_2$ series (see fig. 1 in ref.[9]). The lines (guide for eyes) in fig. 4 show that our samples are in agreement with the expected values considering a linear decrease between extremal x=0 and x=100% compositions. The small deviation from this linear trend (visible in the c-axis variation for $x < 20\%$ for example) is probably due to small variations in iron and/or thallium contents between different samples (see the trend shown in table 1 for refined values of Fe and Tl site occupancy factors). This is also an indication that the description in the average $I4/mmm$ space group is not fully correct and that the real space group should be less symmetric (i.e. taking into account ordered iron vacancies).

In contrast, tellurium substituted samples $Tl_{1-z}Fe_{2-y}(Se_{1-x}Te_x)_2$ show the expected increase of both c-axis, up to c=14.09 Å for x(Te) = 0.5, and a-axis, up to c = 3.94 Å for x(Te) = 0.5 (see left part of fig. 4), considering the larger atomic radius of tellurium compared to the selenium one. The rate of this increase is similar to the one observed in the tetragonal $Fe(Te_{1-x}Se_x)$ series and seems more important for the a-axis than for the c-axis; this trend is opposite to
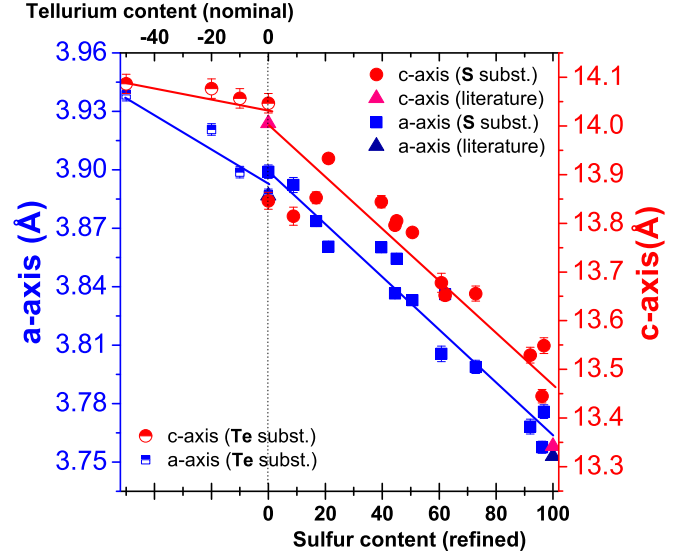
that observed in alkaline-based $Rb_{0.8}Fe_{2-y}(Se_{1-x}Te_x)_2$ series where c-axis increases faster than a-axis with Te content[18].

B. Electron diffraction in TEM

x=0, 0.2 and 0.7 compositions were selected for detailed electron diffraction studies. For the pure selenide (x=0), the EDS analysis carried out on around 50 crystallites shows an homogeneous average cationic composition $TlFe_{1.7}Se_2$, i.e. it contains a significant amount of iron vacancies. The electron diffraction patterns recorded on different particles present a body-centered tetragonal sub-cell with a=b=3.9 Å, c=14 Å. The extinctions observed are compatible with the $I4/mmm$ space group. However, extra reflections, called satellite reflections, can be observed on the [001] oriented basal plane (figure 6). These extra spots are characteristic of a modulated structure with a two-components modulation vector $\vec{q^*} = \alpha\vec{a^*} + \beta\vec{b^*}$. According to this ED pattern, there are several ways to define the modulation vectors. We chose here two vectors in agreement with the superstructure defined previously by Pomjakushin et al.[14] for the Cs-based 122 selenide: $\vec{q_1^*}$ and $\vec{q_2^*}$ lie along [210] and [$\bar{1}$20] directions of the subcell, with an amplitude of 1/5, leading to the values $\vec{q_1^*} = 1/10(-2\vec{a^*}+4\vec{b^*})$ and $\vec{q_2^*} = 1/10(4\vec{a^*}+2\vec{b^*})$. Bearing in mind the commensurate nature of the modulation, the structure can also be described in a supercell a=b=8.7 Å ($=\sqrt{5}$ a), c = 14 Å
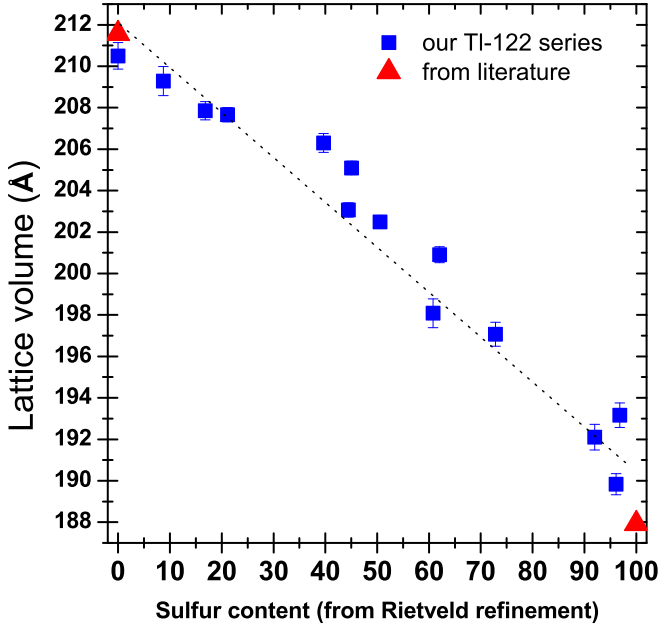
FIG. 5: Sulfur content dependence of the volume lattice in the $Tl_{1-y}Fe_{2-z}(Se_{1-x}S_x)_2$ series.

($I4/m$). This result is in agreement with neutron and x-ray powder and single crystal diffraction data reported recently on $Cs_y Fe_{2-x}Se_2$ system[14] and with the electron diffraction study of $K_y Fe_{2-x}Se_2$ showing evidence of a supercell $\sqrt{5}$ a $\times \sqrt{5}$ a $\times$ c[19].

For a Se-rich composition (x=0.2), the EDS analysis carried out on numerous crystallites confirms a homogeneous cationic composition $Tl_{0.8}Fe_{1.4}Se_{1.5}S_{0.5}$. Note that this sample contains lower contents in thallium and iron than the x=0 sample. The reconstruction of the reciprocal space obtained by tilting around the b* crystallographic axis led to an orthorhombic cell with the parameters a = 5.6 Å ($\sqrt{2}$ a), b = 11.3 Å (2 $\sqrt{2}$ a) and c = 15 Å (figure 7). The reflexions conditions (hkl : h+k+l=2n, 0kl : k = 2n and h0l : h = 2n) are compatible with space group *Ibam* (n$^\circ$ 72). Note that the 101 and 303 reflections visible on the [10$\bar{1}$] ED pattern are artefacts caused by the multiple diffraction ; upon rotation around the [101] axis, these reflections indeed disappear depending on the zone axis. These crystallographic features are in agreement with the indexation of extra weak peaks of the x=0.2 XRD pattern (see fig. 2) , and also with the orthorhombic structure obtained for the $TlFe_{1.5}S_2$ pure sulfide in 1980[20].

For a S-rich system (x=0.7), a very homogeneous cationic composition close to the nominal formulation was revealed by EDS analysis. Electron diffraction evidenced the tetragonal structure as for x=0. Figure 8 exhibits an ED pattern recorded along the [010] zone axis with the parameters $a \sim 3.9$ Å and $c \sim 14$ Å.
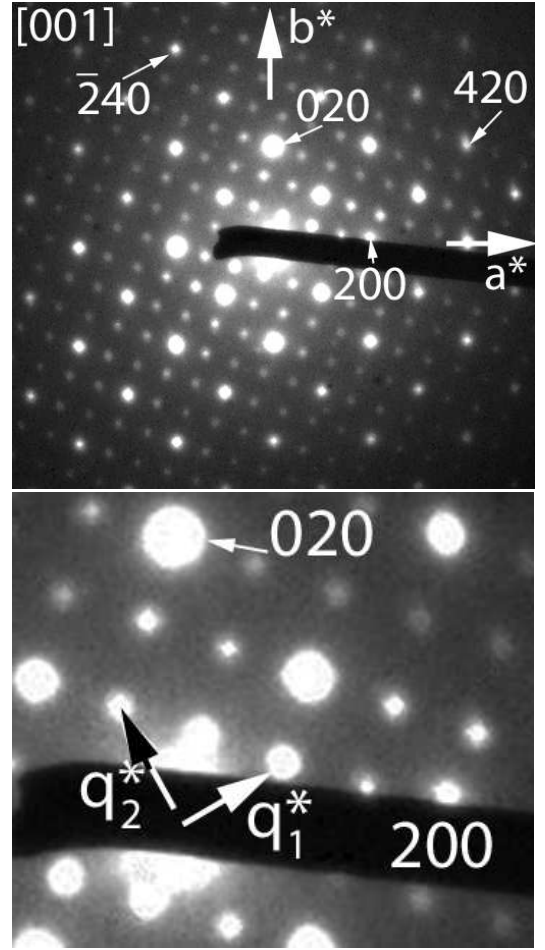

FIG. 6: (Top)[001] ED pattern of x=0 sample ($TlFe_{1.7}Se_2$ from EDS) indexed in a tetragonal sub-cell. (Bottom) The zoomed area evidences the two directions of the modulation vector associated to the satellite reflections.

C. Electrical resistance and magnetization

Figure 9 shows the typical magnetization curve M(T) and electrical resistance R(T) for x=0.2 sample as a function of (high) temperature. We clearly see the onset of the AFM ordering around 390K on the M(T) curve. The appearance of the magnetic ordering corresponds also to an anomaly in the R(T) curve which is more or less marked depending on the sulfur content. This magnetic transition (at T_N) is preceded by a structural transition (at T_S slightly above T_N) which corresponds to the ordering of iron vacancies (disordered at high T, i.e. corresponding to the $I4/mmm$ description), as shown in previous studies by neutron diffraction on $K_{0.8}Fe_{1.6}Se_2$[6] (T_N=559K and T_S=578K) and $Rb_{0.8}Fe_{1.6}Se_2$ (T_N=502K and T_S=515K) or $Cs_{0.8}Fe_{1.6}Se_2$ (T_N=471K and T_S=500K)[16] selenides. In thallium phases T_N and T_S seem to be very close (fig. 9), and we have used the anomaly in the transport measurements as a determination of T_N, as usually
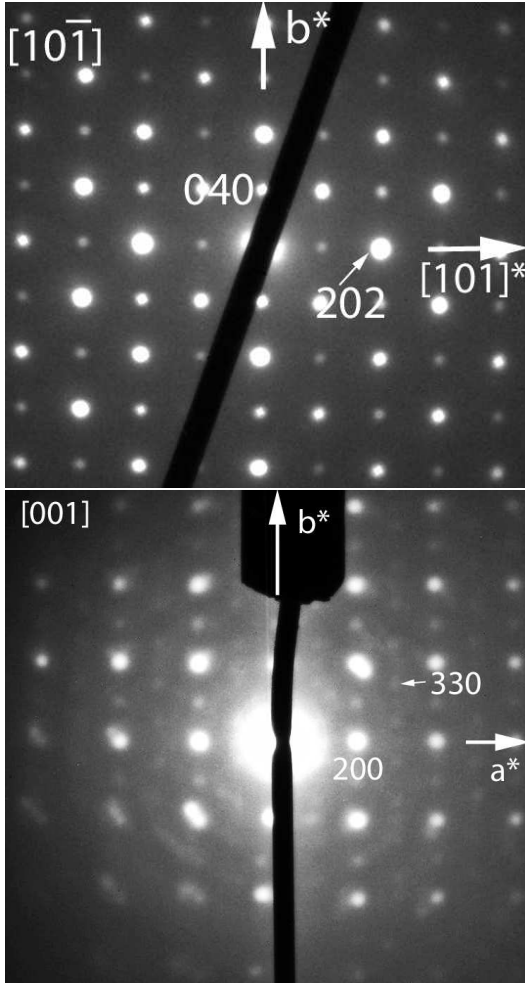
FIG. 7: $[10\bar{1}]$ (top) and [001] (bottom) ED pattern of x=0.2 sample $(Tl_{0.8}Fe_{1.4}(Se_{0.75}S_{0.25})_2$ from EDS) indexed in an orthorhombic cell.

FIG. 8: [010] ED pattern of x=0.7 sample $(Tl_{0.8}Fe_{1.5}(Se_{0.3}S_{0.7})_2$ from EDS) indexed in a tetragonal sub-cell.

FIG. 9: Magnetization measured at 6T and electrical resistance (in log scale) in the 200-500K range of the x=0.2 sample. In both measurement the signature of the onset of the AFM order at T_N is clearly visible.

made in analogous alkaline-based $AFe_{2-y}Se_2$ selenides (A=K,Rb,Cs)[15,22].

The next figure (fig. 10) shows the electrical resistance (R(T)) behaviors (in log scale) of the two extremal composition x=0 and x=1 in a larger temperature range, i.e. from 600K down to the liquid helium temperature. All compositions showed a semi-conducting behavior at low T, independently of the sulfur content. No superconductivity has been found down to 4.2K. In the particular case of the pure selenide (x=0), in the 4-300K range, the R(T) curve of our polycrystalline sample shows two regimes which intersect around T_2=120K, as observed previously by Sales et al. at 100K on a $TlFe_{1.6}Se_2$ single crystal[13]. These authors have also evidenced another transition temperature around T_1=150K, not visible in our samples, based on their specific heat, magnetization and transport measurements. And they have concluded very recently that this particular behavior of $TlFe_{1.6}Se_2$ between T_1 and T_2 was related to a sudden change of z position of 4 Fe spins pointing down (along c-axis) and

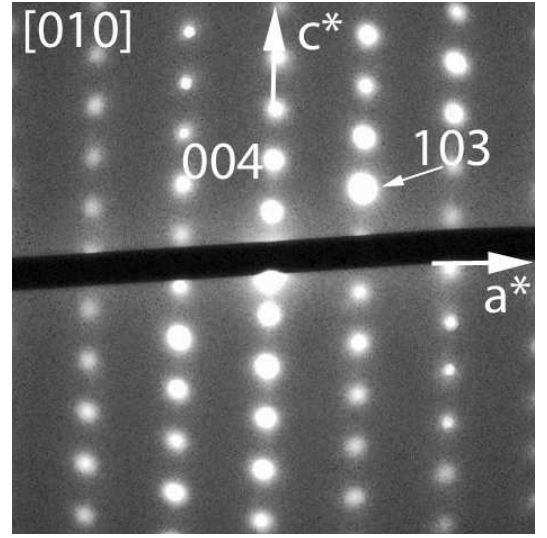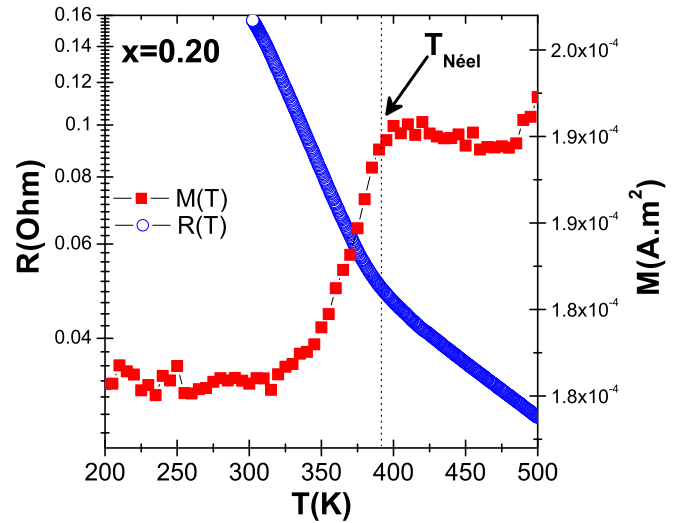4 Fe spins pointing up in the "block checkboard"AFM structure, inducing a corrugation of the iron layer and a canting of the Fe magnetic moment relatively to the c-axis (up to 27(3)° at 115K) for $T_2 < T < T_1$[26]. We are unable with the present data to discuss in details this point, but it seems that T_2 decreases with the sulfur content introduced in the lattice. It will be maybe interesting in the future to study if this unusual magnetoelastic behavior seen in the selenide case for $T_2 < T < T_1$ persists also up to x(S)=1 and how it evolves.
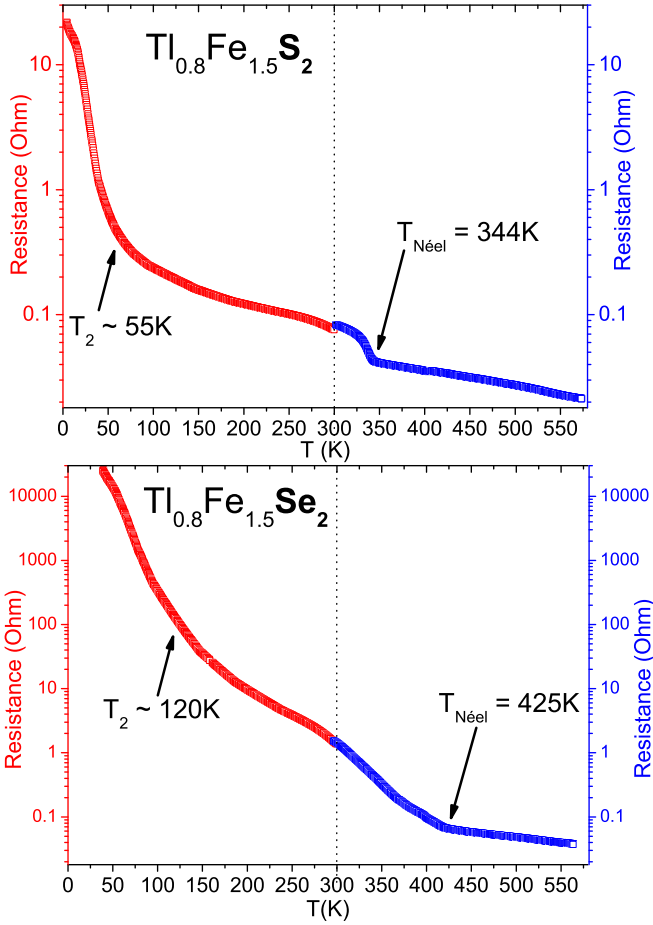
FIG. 10: Low and high temperature dependance of the electrical resistance of typical x=0 and x=1.0 $Tl_{1-y}Fe_{2-z}(Se_{1-x}S_x)_2$ samples emphasizing the signature of the long range AFM structure in the ordered iron vacancies network at T_N.
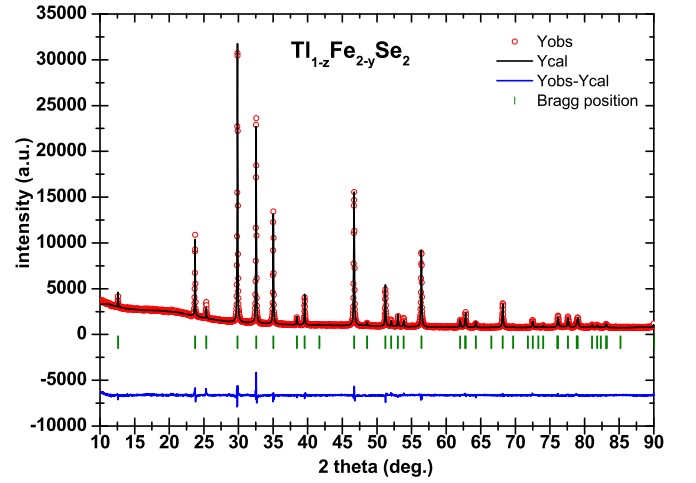

FIG. 11: Rietveld refinement profile of XRD pattern ($\lambda = 1.5406$ Å) for $Tl_{1-z}Fe_{2-y}Se_2$ at room temperature. A difference curve is plotted at the bottom (observed minus calculated). Tick marks correspond to Bragg peaks of 122 selenide in the $I4/mmm$ space group description.

D. Rietveld refinements in the average $I4/mmm$ space group

The structural parameters of $Tl_{1-y}Fe_{2-z}(Se_{1-x}S_x)_2$ were refined from XRD data by the Rietveld method using the "Fullprof" software[23]. Data points with $10° < 2\theta < 90°$ were taken into account. A pseudo-Voigt profile shape was used. The background was fitted using a linear interpolation between selected points.

Attempts to use the space group corresponding to iron vacancy ordering, for instance the tetragonal $\sqrt{5}$ a $\times$ $\sqrt{5}$ a $\times$ c lattice, led to refinement instabilities, due to the weakness of the superstructure reflections. Consequently, all refinements were carried out assuming the tetragonal $I4/mmm$ lattice (space group No.139) i.e. neglecting ordering of iron vacancies.

The structure as described in the $I4/mmm$ space group contains the following Wyckoff sites: Tl at 2a (0,0,0), Fe (in the center of the $FeCh_4$ tetrahedron) at 4d (0,1/2,1/4) and Ch (Ch=Se,S) at 4e (0,0,z) with z $\sim$ 0.355 (with Se and S atoms constrained to the same z coordinate). Refined variables were lattice parameters, the z-position of the chalcogen atom, iron and thallium occupancy factors and (Se,S) occupancy ratio (their total summation was constrained to unity), and all isotropic Debye Waller factors.

Figure 11 illustrates the result of the Rietveld refinement for x=0 (pure selenide) as an example; there is a good agreement between the experimental and the calculated profiles.

Table I. gives the refined structural parameters, bond lengths and angles for x=0, x=0.5 and x=1. Our refined values for extremal x=0 and x=1 compositions are in good agreement with the old (see table I) and very recent

Concerning the high temperature resistivity anomaly associated with the antiferromagnetism ordering below T_N, this characteristic temperature is clearly visible for all x(S) compositions and varies from T_N=450-425K in the selenide (x=0) to T_N=344-330K in the sulfide (x=1).

On the other hand, transport measurements in the $Tl_{1-z}Fe_{2-y}(Se_{1-x}Te_x)_2$ Se-Te system showed superconductivity (with zero resistivity) around T_c=15K (not shown); the corresponding magnetization measurements gave a very small diamagnetic shielding. We therefore conclude that this superconductivity is probably due to the tetragonal $Fe(Te_{1-x}Se_x)$ secondary phase, in agreement with the its fraction estimated from x-ray diffraction. In addition, we note that tellurium substitution in superconducting alkaline-based $Rb_{0.8}Fe_{2-y}(Se_{1-x}Te_x)_2$ induces a strong reduction of superconductivity which disappears for x(Te)=0.15[18].
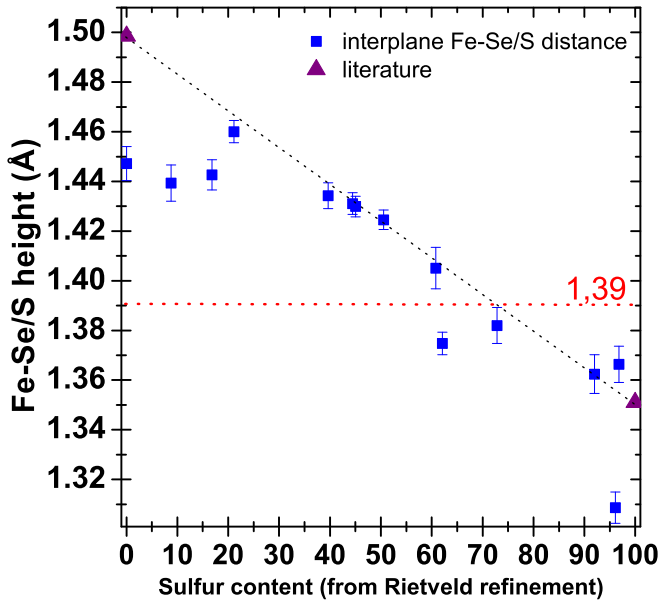
FIG. 12: Fe-(Se,S) height (i.e. interplane Fe-(Se,S) distance) of $Tl_{1-y}Fe_{2-z}(Se_{1-x}S_x)_2$ versus the refined S content.

FIG. 13: Fe-(Se,S) bond length variation in $Tl_{1-y}Fe_{2-z}(Se_{1-x}S_x)_2$ as a function of refined S content.

literature[5,21,26].

Figure 12 shows the evolution of the Fe-(Se,S) height, i.e. the distance between the iron and the (Se,S) planes, with sulfur content. As expected the substitution of Se by S with a smaller atomic radius induces a continuous decrease of this inter-planar distance (from 1.50 Å for x=0 to 1.35 Å for x=1); this distance crosses the ideal value 1.39 Å for which T_c is usually maximal in pnictides[25] and the value 1.41-1.42 Å where T_c is maximal in FeSe under pressure[7]. In a similar way the Fe-(Se,S) bond length decreases regularly with sulfur content in the lattice (see fig. 13) from 2.45 Å in $Tl_{1-y}Fe_{2-z}Se_2$ to 2.30 Å in $Tl_{1-y}Fe_{2-z}S_2$, i.e. covers the range explored under high pressure on pure tetragonal FeSe (2.37 Å at 0 GPa to 2.29 Å at 10 GPa) in which T_c is maximal[3,24]. Nevertheless no superconductivity is observed in our samples down to 4.2K.

Figure 14 shows the variation of the two characteristic (Se,S)-Fe-(Se,S) bond angles in the Fe(Se,S)$_4$ tetrahedron α and β (α notation correspond to two (Se,S) atoms of the same layer, while β notation concerns two (Se,S) atoms on both sides of the iron layer). The two complementary angles merge towards the ideal value of the regular tetrahedron (109.47 deg.), i.e. towards the value for which the maximal T_c is observed in superconducting iron-based arsenides. Again, despite this, no superconductivity is found for any (Se,S) composition.

It should be pointed out that the maximal T_c value is not achieved in FeSe iron selenide when the angle is ideal; on the contrary T_c values above 30K are reached for strongly distorted tetrahedron[3,24].
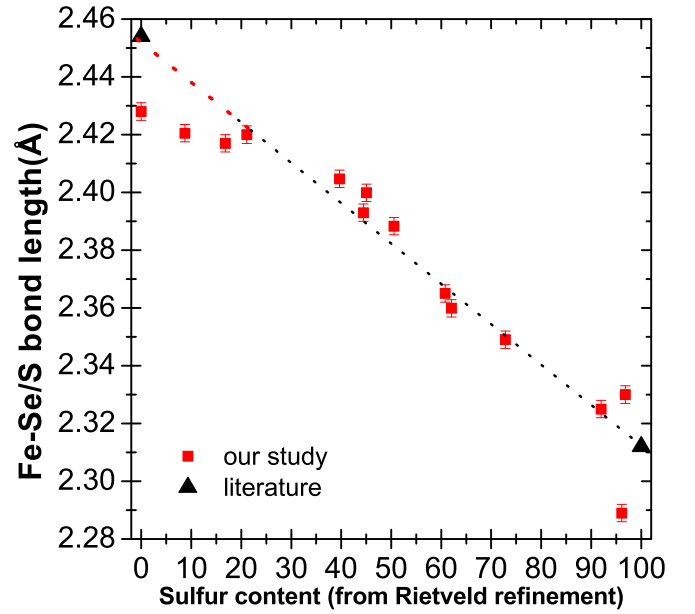

FIG. 14: (Se,S)-Fe-(Se,S) bond angle in the Fe(Se,S)$_4$ tetrahedron in $Tl_{1-y}Fe_{2-z}(Se_{1-x}S_x)_2$ as a function of refined S content.

E. Discussion

Rietveld refinements evidenced the continuous decrease of both Fe-(Se,S) bond length and Fe-(Se,S) height with sulfur content in $Tl_{1-y}Fe_{2-z}(Se_{1-x}S_x)_2$. As pointed out above, despite the evolution of the structural parameters towards values usually favoring superconductivity (i.e. optimal Fe-Ch height and optimal Ch-Fe-Ch angle), superconductivity is not induced by isovalent substitu-

TABLE I: Refined structural parameters of x=0, x=0.5 and x=1 compositions of $Tl_{1-y}Fe_{2-z}(Se_{1-x}S_x)_2$ series using the average $I4/mmm$ description (Ch=Se,S).

compound	x=0 Häggström et al.[5] (1986)	x=0 at 250K Cao et al.[26] (2012)	x=0	x=0.5	x=1	x=1 Klepp and Boller [21] (1978)
a-axis (Å)	3.8867(3)	3.884(2)[d]	3.8870(1)	3.8331(2)	3.7572(3)	3.755(1)
c-axis (Å)	14.005(1)	14.002(7)	14.0401(3)	13.781(1)	13.443(2)	13.35(1)
n(Tl)	1	1	0.98(2)	0.90(2)	0.92(2)	1
n(Fe)	1	0.795(5)[e]	0.66(2)	0.71(1)	0.70(1)	1
n(S)	-	-	-	0.52(2)	1	1
z(Ch)	0.357[a]	0.3575(2)[f]	0.3530(2)	0.3541(2)	0.3478(5)	0.3600
Fe-(Ch) height (Å)	1.50(1)	1.505(7)	1.446(3)	1.434(3)	1.315(5)	1.46(1)
Fe-(Ch) bond length (Å)	2.457(1)	2.457(2)	2.422(2)	2.394(2)	2.294(4)	2.334(1)
(Ch)-Fe-(Ch) bond angle (deg.)	104.55[b]	104.44(1)	106.70(5)	106.37(8)	110.0(1)	107.1(1)
Rp (%)	-[c]	R_1=5.89	21.3	18.0	24.7	-[a]
Rwp (%)	-[c]	wRF^2=13.2	14.6	13.2	20.2	-[a]
Chi²	-[c]	8.04	3.25	0.478	4.86	-[a]

[a] parameter fixed; [b] calculated; [c] not given in the paper.
[d] from neutron diffraction on single crystal in $I4/m$ supercell; a-axis was divided by $\sqrt{5}$ for the comparison; [e] average value of total Fe1 (16i) and Fe2 (4d) site occupancies calculated taking into account the multiplicity of both iron sites; [f] average z-positions of Se1 (4e) and Se2 (16i) calculated taking into account the multiplicity of both selenium sites.

tion of selenium by sulfur in this iron-deficient Tl-122 system. Nevertheless it has been reported that partial replacement of Tl by an alkaline element leads to the appearance of superconductivity[27], with T_c around 30K.

This difference of behavior could be related to slight structural differences between thallium and alkaline element systems. First of all, the lattice volume, and then lattice parameters, of the Tl-122 selenide are smaller than those of analogous compounds with A=K,Rb,Cs by about $1-2\%$ (see table 1 in ref[16] for a comparison). Secondly, the relative position of the chalcogen atom relatively to the iron plane in the 122 selenides varies: z=0.3530(2) in Tl-122 (this work) compared to z=0.3539(2)[1]-0.3560(3)[28] in K-122 and z=0.3439(3)[28]-0.3456(4)[14] in Cs-122. This induces slightly shorter Fe-Se and Fe-Fe bond lengths in the Tl-122 compared to A-122 (A=K,Rb,Cs) by $1-2\%$. These differences are enhanced when Se is substituted by S in Tl-122, and this could affect the electronic structure, and consequently the insulating/superconducting behavior at low T.

The first DFT calculation was performed on stoichiometric hypothetical $TlFe_2Se_2$ and revealed that the Fermi surface is relatively close to the other iron-based compounds, i.e. contains two electron cylinders, but with hole surfaces suppressed[29]. Electronic structure calculations were then carried out on more realistic compositions: z=0.5 (with orthorhombic $\sqrt{2}$ a $\times 2\sqrt{2}$ a $\times$ c superstructure) and z=0.4 (with tetragonal $\sqrt{5}$ a $\times\sqrt{5}$ a $\times$ c supercell) and compared with alkaline-based analogous selenides[30–32]. In particular, it was found that the Fermi surface of $TlFe_{1.6}Se_2$ is in fact highly three-dimensional, unlike alkaline-based selenides[32]. Moreover, in the early calculations for z=0 (i.e. without iron vacancies), the density of states at the Fermi level $N(E_F)$ was found to decrease from 3.6-3.94 states/(eV.cell) in Cs or

K intercalated selenides[33,34] to ca. 2 states/(eV.cell)[29] in Tl-122 selenide. On the other hand, the full replacement of Se by S in K-122 was found to reduce $N(E_F)$ by ca. 50% to 2.025 states/eV/cell for KFe_2S_2[34]. This lower $N(E_F)$ in the Tl-based selenide, and even lower $N(E_F)$ with S substitution, could explain why x=0 and all S-substituted samples of the $Tl_{1-y}Fe_{2-z}(Se_{1-x}S_x)_2$ series are not superconducting at low temperature. This hypothesis has to be checked theoretically (using realistic crystallographic structures determined experimentally for the electronic structure calculations) and experimentally. In that sense ARPES measurements on pure thallium-based chalcogenides would be very useful.

Another important issue, still under debate, is the possible existence of chemical/electronic phase separation at the nanoscale in $A_{0.8}Fe_{2-z}Se_2$ selenides (A=K,Rb,Cs) suggested by TEM structural studies[19], synchrotron XRD[35] or STM studies of K-122 films[36]. Very recently, based on back-scattered electron images (SEM) and Mössbauer spectroscopy Hu. et al. suggested that superconductivity of $K_{0.8}Fe_{1.76}Se_2$ may be due to a submicron phase of $K_{0.6}Fe_{1.9}Se_2$ composition[37]; Texier et al. also reported a phase separation in a $Rb_{0.74}Fe_{1.6}Se_2$ single crystal studied by NMR and attributed superconductivity to the $Rb_{0.3(1)}Fe_2Se_2$ phase[38]. In the case of Tl-based 122 selenides, no phase separation has been reported in the literature up to now; Tl intercalated selenides appear more homogeneous, with a constant iron content distribution and a nearly full Tl site, i.e. z=0-0.1 (contrary to A-122 selenides for which the alkaline site is more deficient: z=0.2). All these results seem to imply that the doping level (then the iron valency) is very different between the actual superconducting A-122 phases and the Tl-122(Se,S) series, and this could also explain why superconductivity is not observed in Tl-122(Se,S)

compounds.

Addressing now the high temperature magnetic behavior of the Tl-122(Se,S) series, we have plotted Néel temperature values (T_N) extracted from our transport measurements (see fig. 10) vs the sulfur content x(S)in fig. 15. It shows a regular decrease of T_N with S content. As a consequence, there is a very good correlation between T_N and the Fe-(Se,S) height (see fig. 16): T_N decreases continuously with the decrease of the Fe-(Se,S) height. A similar trend is observed for a plot of T_N as a function of the Fe-(Se,S) bond length (not shown).

We note that an opposite behavior has been reported in LaFeAsO when As is substituted isoelectronically by Sb: T_N decreases also monotonously with antimony substitution, corresponding to an increase of the equivalent Fe-(As,Sb) bond length[39]. This behavior results from a complex competition between different magnetic interactions in the system, i.e. the relative magnetic exchange integrals between nearest iron neighbors and next-nearest iron atoms in the same iron plane on one hand, and the magnetic exchange between iron atoms from different planes on the other. More theoretical work is necessary to interpret this linear correlation with S content, determine the different magnetic interaction energies and find the most stable magnetic configuration. The related calculations were already made for the z=0.4 and z=0.5 (y=0 in both cases) compositions[30,32]. It would be useful to extend it to sulfur-substituted compositions. In addition it would also be interesting to study the evolution magnetic excitations with sulfur content in the thallium-based series and the differences with respect to their superconducting alkaline-based analogues. In view of this, we performed preliminary neutron diffraction experiments on Tl-122(Se,S) to investigate their static long-range magnetic structure. The results of this work will be published elsewhere.

IV. CONCLUSION

The full solid solution of the $Tl_{1-y}Fe_{2-z}(Se_{1-x}S_x)_2$ series, i.e. from x=0 to x=1 was synthesized using the sealed tube technique. The equivalent series with Se substituted by Te was also synthesized up to x(Te)=0.5, but above x(Te)=0.25 samples were not monophasic. The sulfur-based series was particularly studied by x-ray diffraction, electron diffraction, magnetization and transport measurements. No superconductivity was found down to 4.2K despite that the optimal crystallographic parameters are reached in the S-based series (i.e. the Fe-(Se,S) height and (Se,S)-Fe-(Se,S) angle for which the critical superconducting transition T_c is usually maximal in pnictides). For Te-substituted samples we note superconducting transitions, but probably related to the tetragonal Fe(Te,Se) impurity phase. The S-based solid solution shows a decrease of its Néel temperature (T_N), indicating the onset of the antiferromagnetism order, from 450K in the selenide (x=0) to 330K in the sulfide
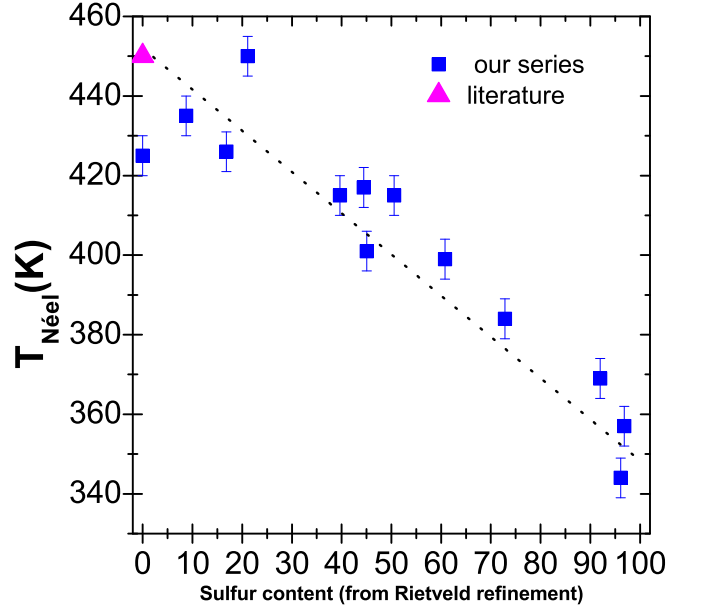

FIG. 15: Néel temperature (extracted from the electrical resistance measurement) in $Tl_{1-y}Fe_{2-z}(Se_{1-x}S_x)_2$ samples versus the refined S content.
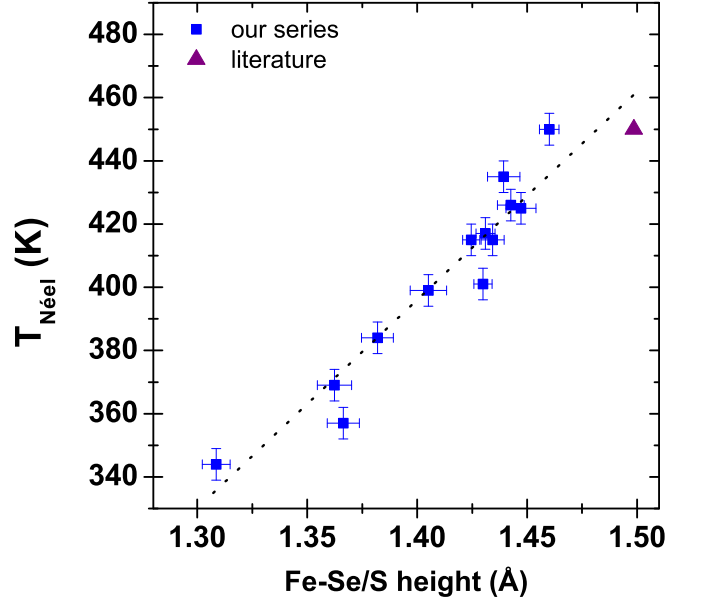

FIG. 16: Néel temperature in our $Tl_{1-y}Fe_{2-z}(Se_{1-x}S_x)_2$ samples as a function of the Fe-(Se,S) height in the structure.

(x=1). Our structural investigation emphasizes a direct linear relationship between T_N and the Fe-(Se,S) bond length.

* Corresponding author. Fax: 00334 7688 1038, e-mail: pierre.toulemonde@grenoble.cnrs.fr

[1] J. Guo, S. Jin, G. Wang, S. Wang, K. Zhu, T. Zhou, M. He, and X. Chen , Phy. Rev. B **82**, 180520(R) (2010).

[2] Y. Mizuguchi, F. Tomioka, S. Tsuda, T. Yamaguchi, and Y. Takano, Appl. Phys. Lett. **93**, 152505 (2008).

[3] G. Garbarino, A. Sow, P. Lejay, A. Sulpice, P. Toulemonde, M. Mezouar, M. Núñez-Regueiro, Euro. Phys. Lett. **86**, 27001 (2009).

[4] S. Medvedev, T.M. McQueen, I.A. Troyan, T. Palasyuk, M. I. Eremets, R. J. Cava, S. Naghavi, F. Casper, V. Ksenofontov, G.Wortmann and C. Felser, Nature Mat. **8**, 630 (2009).

[5] L. Häggström, H.R. Varma, B. Bjarman, R. Wäppling, and R. Berger, J. Sol. St. Chem. **63**, 401-408 (1986).

[6] W. Bao, Q.Z. Huang, G.F. Chen, M.A. Green, D.M. Wang, J.B. He and Y.M. Qiu, Chin. Phys. Lett. **28**, 086104 (2011).

[7] H. Okabe, N. Takeshita, K. Horigane, T. Muranaka, and J. Akimitsu, Phys. Rev. B. **81**, 205119 (2010).

[8] C.H. Lee, A. Iyo, H. Kito, M.T. Fernandez-Diaz, T. Ito, K. Kihou, H. Mastsuhata, M. Braden, and K. Yamada, J. Phys. Soc. Jap. **77**, 083704 (2008).

[9] H. Lei, M. Abeykoon, E.S. Bozin, K. Wang, J. B. Warren, and C. Petrovic, Phys. Rev. Lett. **107**, 137002 (2011).

[10] T. Klein, D. Braithwaite, A. Demuer, W. Knafo, G. Lapertot, C. Marcenat, P. Rodière, I. Sheikin, P. Strobel, A. Sulpice, and P. Toulemonde, Phys. Rev. B, **82**, 184506 (2010).

[11] Y. Noat, T. Cren, V. Dubost, S. Lange, F. Debontridder, P. Toulemonde, J. Marcus, A. Sulpice, W. Sacks, and D. Roditchev, J. Phys. Condens Mat **22**, 465701 (2010).

[12] H. Sabrowsky, M. Rosenberg, D. Welz, P. Deppet, W. Schäfer, J.Magn. Magn. Mat. **54-57**, 1497-1498 (1986).

[13] B. Sales, M.A. McGuire, A.F. May, H. Cao, B.C. Chakoumakos, and A.S. Sefat, Phys. Rev. B. **83**, 224510 (2011).

[14] V. Yu. Pomjakushin, D. V. Sheptyakov, E. V. Pomjakushina, A. Krzton-Maziopa, K. Conder, D. Chernyshov, V. Svitlyk, and Z. Shermadini, Phys. Rev. B **83**, 144410 (2011).

[15] Y.J. Song, Z. Wang, Z.W. Wang, H.L. Shi, Z. Chen, H.F. Tian, G.F. Chen, H.X. Yang, and J.Q. Li, Euro.Phys.Lett **95**, 37007 (2011).

[16] F. Ye, S. Chi, W. Bao, X.F. Wang, J.J. Ying, X.H. Chen, H.D. Wang, C.H. Dong, and M. Fang, Phys. Rev. Lett. **107**, 137003 (2011).

[17] P. Zavalij, W. Bao, X.F. Wang, J.J. Ying, X.H. Chen, D.M. Wang, J.B. He, X.Q. Wang, G.F. Chen, P.-Y. Hsieh, Q. Huang, and M.A. Green, Phys. Rev. B **83**, 132509 (2011).

[18] D. Gu, L. Sun, Q. Wu, C. Zhang, J. Guo, P. Gao, Y. Wu, X. Dong, X. Dai, Z. Zhao, arXiv:1107.4719 (2001).

[19] Z. Wang, Y. J. Song, H. L. Shi, Z. W. Wang, Z. Chen, H. F. Tian, G. F. Chen, J. G. Guo, H. X. Yang, and J. Q. Li, Phys. Rev. B **83**, 140505(R) (2011).

[20] M. Zabel, K-J Range, Revue de Chimie Générale, 17, 561 (1980).

[21] K.O. Klepp, and H. Boller, Monatshefte fuer Chemie und verwandte Teile anderer Wissenschaften **109**, 1049 (1978).

[22] R. H. Liu, X. G. Luo, M. Zhang, A. F. Wang, J. J. Ying, X. F. Wang, Y. J. Yan, Z. J. Xiang, P. Cheng, G. J. Ye, Z. Y. Li and X. H. Chen, Euro. Phys. Lett. **94**, 27008 (2011).

[23] J. Rodrguez-Carvajal, Physica B 192, 55 (1993).

[24] S. Margadonna, Y. Takabayashi, Y. Ohishi, Y. Mizuguchi, Y. Takano, T. Kagayama, T. Nakagawa, M. Takata, and K. Prassides, Phys. Rev. B **80**, 064506 (2009).

[25] G. Garbarino, R. Weht, A. Sow, A. Sulpice, P. Toulemonde, M. A lvarez-Murga, P. Strobel, P. Bouvier, M. Mezouar, and M. Núñez-Regueiro, Phys. Rev. B **84**, 024510 (2011). B 85,

[26] H. Cao, C. Cantoni, A.F. May, M.A. McGuire, B.C. Chakoumakos, S.J. Pennycook, R. Custelcean, A.S. Sefat, and Brian C. Sales, Phys. Rev. B **85**, 054515 (2012).

[27] M.H. Fang H.D. Wang, C.H. Dong, Z.J. Li, C.M. Feng, J. Chen, and H.Q.Yuan, Euro. Phys. Lett. **94**, 27009 (2011).

[28] A. Krzton-Maziopa, Z. Shermadini, E. Pomjakushina, V. Pomjakushin, M. Bendele, A Amato, R. Khasanov, H. Luetkens and K. Conder, J. Phys.: Condens. Matter **23** 052203 (2011).

[29] Lijun Zhang and D. J. Singh, Phys. Rev. B **79**, 094528 (2009).

[30] X.W. Yan, M. Gao, Z.Y. Lu, and T. Xiang, Phys. Rev. Lett. **106**, 087005 (2011).

[31] C. Cao and J. Dai, Phys. Rev. B **83**, 193104 (2011).

[32] C. Cao and J. Dai, Phys. Rev. Lett. **107**, 056401 (2011).

[33] I.A. Nekrasov and M.V. Sadovskii, JETP Letters **93**, 166 (2011).

[34] I.R. Shein and A.L. Ivanovskii, J. Supercond. Nov. Magn. **24** 2215 (2011).

[35] A. Ricci, N. Poccia, G. Campi, B. Joseph, G. Arrighetti, L. Barba, M. Reynolds, M. Burghammer, H. Takeya, Y. Mizuguchi, Y. Takano, M. Colapietro, N. L. Saini, and A. Bianconi, Phys. Rev. B **84**, 060511(R) (2011).

[36] W.Li, H. Ding, P. Deng, K. Chang1, C. Song, Ke He, Lili-Wang, X. Ma, J.-P. Hu, Xi Chen, and Qi-K. Xue, Nat. Phys.**8**, 126 (2012).

[37] R. Hu et al., to be a chapter in the book titled "Iron Pnictide Superconductors: materials, properties and mechanism" by Pan Stanford Publishing, arXiv:1201.0953 (2012).

[38] Y. Texier, J. Deisenhofer, V. Tsurkan, A. Loidl, D. S. Inosov, G. Friemel, and J. Bobroff, arXiv:1201.0953 (2012).

[39] S. J. E. Carlsson, F. Levy-Bertrand, C. Marcenat, A. Sulpice, J. Marcus, S. Pairis, T. Klein, M. Nunez-Regueiro, G. Garbarino, T. Hansen, V. Nassif, and P. Toulemonde,

Phys. Rev. B **84**, 104523 (2011).